Article

Enhanced Photocatalytic Degradation of P-Chlorophenol by ZnIn$_2$S$_4$ Nanoflowers Modified with Carbon Quantum Dots

Jinli Qiu [1], Quan Liu [2], Yixing Qiu [2], Fuqiang Liu [2,*] and Fenghe Wang [1]

[1] School of the Environment, Nanjing Normal University, Nanjing 210023, China
[2] School of the Environment, Nanjing University, Nanjing 210023, China
* Correspondence: lfq@nju.edu.cn

Abstract: The removal of chlorophenol (CP) contaminants from water is a great challenge owing to their natural robustness and the toxic chlorinated by-products generated in degradation processes. In this work, a series of three-dimensional nanoflower-like structured photocatalysts (CQDs/ZnIn$_2$S$_4$-x, x = 1, 2, or 3 wt%) were fabricated via a facile hydrothermal approach. Excellent photocatalytic abilities toward 4-CP degradation under Xe lamp irradiation were achieved over the as-prepared composites. The removal efficiency of total organic carbon for 4-CP on the optimized CQDs/ZnIn$_2$S$_4$-2 was 49.1%, which was 16.0% higher than that of ZnIn$_2$S$_4$. The presence of CQDs could not only be used to adjust controllable band structures for enhancing light absorption, but it could also serve as an electron acceptor to promote the transition of electron–hole pairs. Moreover, a possible degradation mechanism of 4-CP was also proposed according to the analyses of active species, electron paramagnetic resonance characterization, degradation products, and attacked sites. Overall, this work unveils a superior function of an efficient photocatalyst for refractory organic pollutants.

Keywords: photocatalysis; 4-CP; CQDs; ZnIn$_2$S$_4$

1. Introduction

Chlorophenols (CPs) are one of the most harmful persistent pollutants and are widely used as pesticides and disinfectants [1–3]. Strong conjugate interactions between the aromatic nucleus and Cl have structurally endowed CPs with high stability and toxicity. Owing to their carcinogenicity, mutagenicity, and adverse ecosystem effects, CPs have been defined as priority organic pollutants by the U.S. Environmental Protection Agency [4,5]. Therefore, it is of great importance to develop advanced techniques for the treatment of CPs. Recently, advanced oxidation processes (AOPs), including the electrochemical method, Fenton treatment, and persulfate oxidation, have increasingly emerged for the removal of CPs [6–8]. Although the CPs could be degraded by the above technologies, their dissatisfactory selectivity could result in the generation of harmful organic Cl byproducts, further resulting in secondary environmental risks. Thus, it is necessary to develop an inexpensive and green method for the complete degradation of CPs. Heterogeneous photocatalysis technologies have drawn more and more attention due to their advantages of mild reaction conditions and low energy consumption [9,10]. Nevertheless, the fairly high photo-induced carrier combination rate and weak visible light adsorption ability limit their further applications. Therefore, designing photocatalysts with high activity is a great challenge.

ZnIn$_2$S$_4$, a ternary chalcogenide, is considered as a potential photocatalyst owing to its appropriate band gap (~2.4 eV) and superior visible light absorption capacity [11,12]. However, the high recombination rate of photo-generated carriers is the key bottleneck of ZnIn$_2$S$_4$ [13]. Decorating ZnIn$_2$S$_4$ with other semiconductor photocatalysts or noble metals, such as TiO$_2$, MoS$_2$, and Ag NPs, is an efficient strategy to improve the separation efficiency of electron–hole pairs [14–16]. Compared with the above materials,

carbon quantum dots (CQDs), as a typical carbon nanomaterial with sizes no larger than 10 nm [17,18], have attracted extensive attention due to their advantages, such as abundant functional groups, low cost, outstanding optical properties, environmental friendliness, and facile synthesis [19–21]. Benefiting from their superior electrochemical properties, they have drawn extensive attention in photocatalysis. It is worth noting that CQDs can act as electron acceptors, facilitating electron transfer and notably improving charge separation and light absorption. Furthermore, the upconversion characteristics of CQDs also favor the broadening of the light absorption range.

Inspired by the above discussion, the design of CQD-modified photocatalytic composites is beneficial for achieving excellent photocatalytic performance for pollutant elimination. Therefore, in this work, nanoflower-like CQDs/ZnIn$_2$S$_4$-x (x = 1, 2, or 3 wt%) composites were fabricated by a simple hydrothermal method, which was employed to degrade p-chlorophenol (4-CP) under Xe lamp irradiation. The synthetic parameters of CQDs/ZnIn$_2$S$_4$-x were also optimized by investigating their photocatalytic activities toward 4-CP. The effects of different reaction conditions, including the initial pH, catalyst concentration, and co-existing inorganic anions, were investigated. In addition, the catalyst's stability, degradation pathways, photocatalytic mechanism, and variations in the toxicity of 4-CP were systematically explored.

2. Results and Discussion

2.1. Characterization and Performance Valuation

A scanning electron microscope (SEM) was employed to observe the surface morphology of the as-prepared materials. Figure 1a,b exhibits a three-dimensional nanoflower-like structure of ZnIn$_2$S$_4$, which was assembled by a series of nanosheets. However, the surface morphology of CQDs could not be observed from the SEM result. Herein, high-resolution transmission electron microscopy (HRTEM) and the corresponding energy dispersive spectrometer (EDS) elemental mapping of CQDs/ZnIn$_2$S$_4$-2 were further carried out. As depicted in Figure 1c–h and Figure S1, the CQDs and elements, including Zn, In, S, and C, could be clearly observed.
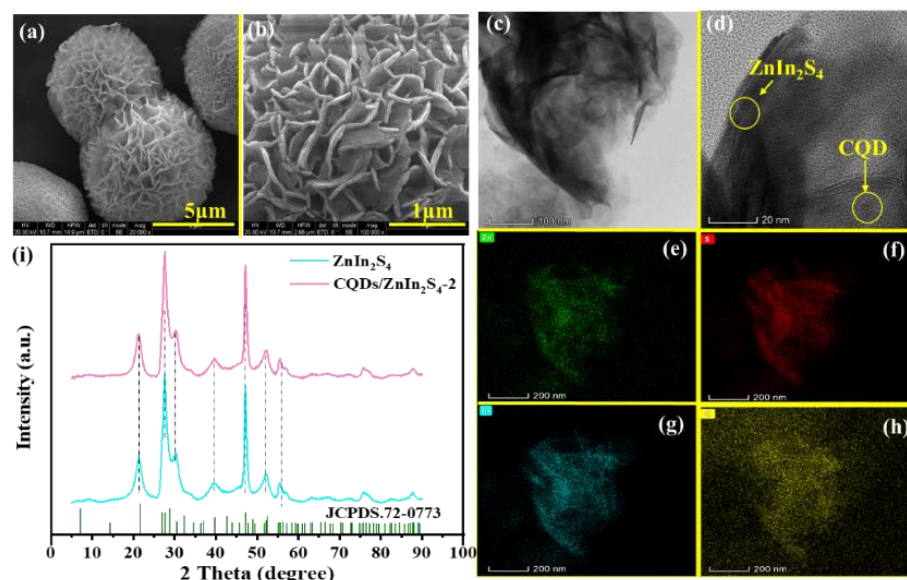

Figure 1. SEM images with different scales: 5 μm (**a**) and 1 μm (**b**); HRTEM images with different scales: 100 nm (**c**) and 20 nm (**d**); EDS elemental mapping images of C, Zn, In, and S elements (**e**–**h**); and XRD patterns of the as-prepared samples (**i**).

The crystal type and crystallinity of ZnIn$_2$S$_4$ and CQDs/ZnIn$_2$S$_4$-2 were measured by X-ray electron diffraction (XRD), and the results are shown in Figure 1i. The peaks at 2θ = 21.8°, 27.6°, 30.5°, 39.8°, 47.1°, 52.3°, and 55.4° were indexed to the (006), (102),

(104), (108), (110), (116), and (022) planes of hexagonal $ZnIn_2S_4$ (JCPDS No. 72-0773), respectively [22]. However, no obvious diffraction peaks of CQDs could be observed in CQDs/$ZnIn_2S_4$-2, which may be due to the low amount of CQDs in the composite. An X-ray photoelectron spectrum (XPS) was employed to analyze the chemical composition and chemical state of the as-prepared CQDs/$ZnIn_2S_4$-2. As depicted in Figure 2a, the Zn 2p spectrum of CQDs/$ZnIn_2S_4$-2 exhibited two distinct peaks at 1022.0 eV and 1045.1 eV, which corresponded to Zn $2p_{3/2}$ and Zn $2p_{1/2}$, respectively. Meanwhile, the peaks at the binding energies of 445.1 and 452.8 eV belonged to In $3d_{5/2}$ and In $3d_{3/2}$, respectively (Figure 2b) [23]. As presented in Figure 2c, the S 2p spectrum of CQDs/$ZnIn_2S_4$-2 could be fitted into two peaks at 162.0 and 163.1 eV, which were ascribed to S $2p_{3/2}$ and S $2p_{1/2}$, respectively. Figure 2d shows the C1s spectrum of CQDs/$ZnIn_2S_4$-2; the binding energies at 284.6 eV, 285.8 eV, and 289.0 eV were attributed to the C–C/C=C, C-O, and C=O bonds, respectively. These results confirmed the successful preparation of CQDs/$ZnIn_2S_4$-2.
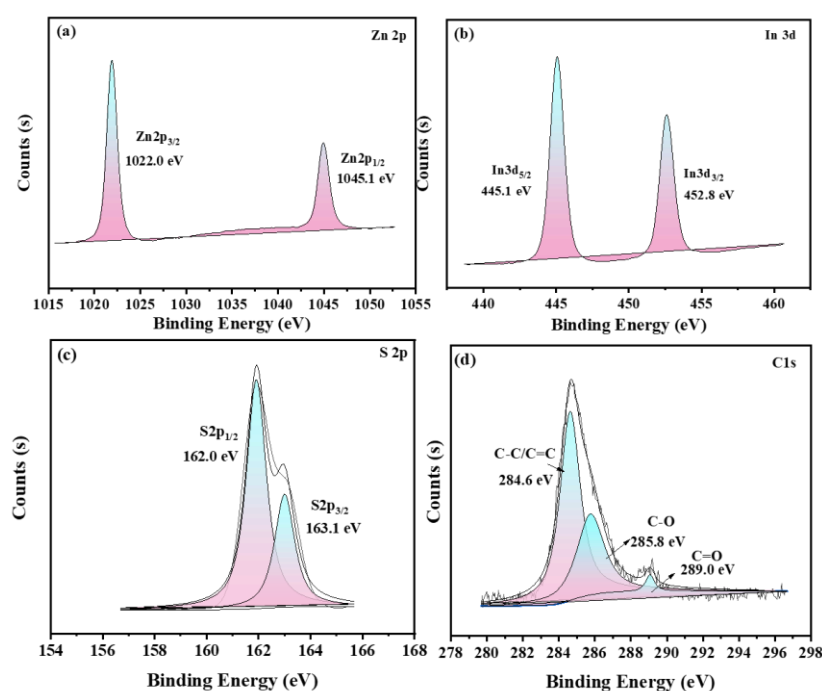

Figure 2. XPS spectra of the CQDs/$ZnIn_2S_4$-2: high-resolution scans of (**a**) Zn 2p, (**b**) In 3d, (**c**) S 2p, and (**d**) C 1s.

Photoelectrochemical measurements, including UV-vis diffuse reflectance spectra (UV-vis DRS), photocurrent, and electrochemical impedance spectroscopy (EIS), were carried out to prove the positive roles of CQDs for improving the photocatalytic drawbacks of $ZnIn_2S_4$ [24–26]. The photocurrent response of CQDs/$ZnIn_2S_4$-2 was observably enhanced due to the introduction of CQDs (Figure 3a), which indicated the more efficient charge separation efficiency of the CQDs/$ZnIn_2S_4$-2 composite. The result (Figure S2) of UV-vis DRS demonstrated the enhanced light adsorption ability of CQDs/$ZnIn_2S_4$-2. Moreover, as presented in Figure 3b, the semicircle of CQDs/$ZnIn_2S_4$-2 was smaller than that of pure $ZnIn_2S_4$, suggesting its excellent electron mobility rate, and the larger slope of the line part indicated its low charge transfer resistance. The synthetic parameters of photocatalysts may notably affect their activities. Therefore, the photocatalytic activities of CQDs/$ZnIn_2S_4$-x (x = 1, 2, or 3 wt%) with different loading amounts of CQDs were investigated through the degradation of 4-CP under Xe lamp irradiation. As presented in Figures 3 and S3, the CQDs/$ZnIn_2S_4$-2 exhibited the optimal degradation performance for 4-CP. This indicates that the suitable loading of CQDs could improve the degradation performance of 4-CP. However, the excessive CQDs could cover the active sites on the surface of the CQDs/$ZnIn_2S_4$-x composite. Furthermore, the total organic carbon (TOC)

removal efficiency for 4-CP on CQDs/ZnIn$_2$S$_4$-2 was 49.1%, which was 16.0% higher than that of ZnIn$_2$S$_4$ (Figure S4). The effect of the pH value (3, 5, 7, and 9) on 4-CP degradation was determined and is given in Figure S5. It can be seen that the degradation rate of 4-CP was not clearly affected under neutral and alkaline conditions, which confirmed that an alkaline environment was more favorable for 4-CP degradation. The effect of the catalyst dosage was also studied. As presented in Figure S6, the removal rate of 4-CP increased significantly with the increase in the catalyst concentration (0.25 to 0.375 g/L), which may have benefitted from the increase in the number of active sites. However, the removal rate of 4-CP could not be further enhanced when the catalyst dosage was 0.625 g/L, which was possibly due to the shielding effect of overloading the catalyst, and thus weakened the penetration of light. Inorganic anions in natural water could affect the degradation performance of a pollutant. Herein, the effect of anions, including Cl$^-$, SO$_4^{2-}$, and NO$_3^-$, was investigated. As can be seen from Figure S7, the co-existing inorganic anions had no obvious effects on the decomposition of 4-CP. The reusability and stability of photocatalysts were crucial factors for evaluating their potential in practical applications. Therefore, in this study, four consecutive cycles for the photocatalytic degradation of 4-CP were performed. After four cycles, the degradation efficiency of 4-CP only decreased by 7.6% (Figure 3d), indicating its good reusability and stability. Meanwhile, it can be seen that the peak of the XRD spectrum over CQDs/ZnIn$_2$S$_4$-2 exhibited no obvious change after the cycling experiment, further proving its excellent stability (Figure S8). The degradation performance of the as-prepared catalyst was compared with the previously reported literature presented in Table S1. It could be confirmed that the degradation performance of the CQDs/ZnIn$_2$S$_4$-2 synthesized in this study was better than those of previously reported catalysts.
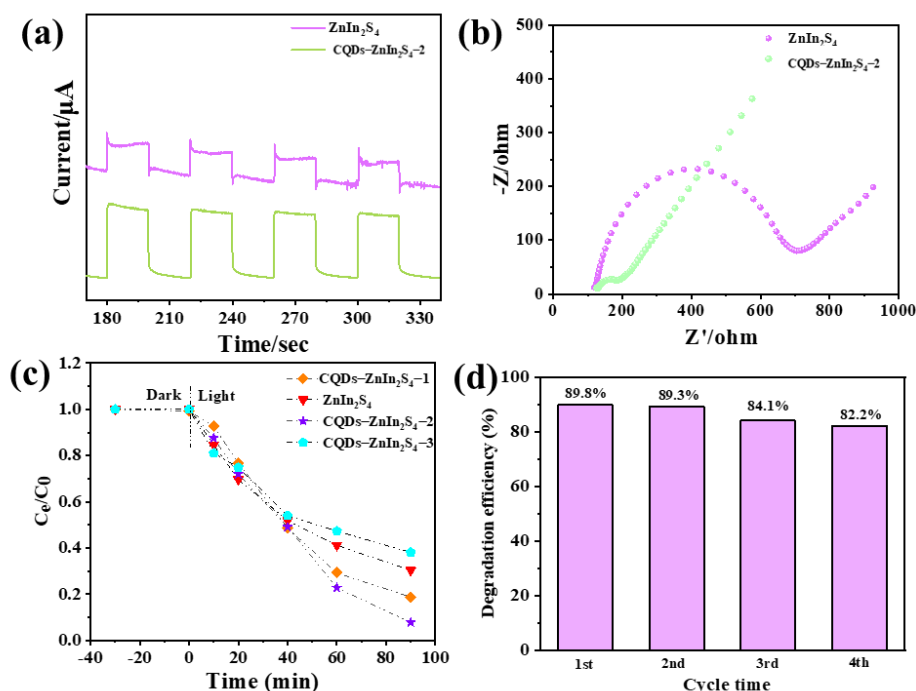

Figure 3. (**a**) Transient photocurrent spectra; (**b**) EIS spectra of the as-prepared samples; (**c**) photocatalytic performance of 4-CP degradation on different photocatalysts; and (**d**) cycling experiments of photocatalytic activity evaluation on CQDs/ZnIn$_2$S$_4$-2.

Free radical capture experiments were conducted to investigate the active species in the photocatalytic system. Generally, EDTA (ethylene diamine tetraacetic acid), NBT (nitroblue tetrazolium), and IPA (isopropanol) were employed as the scavengers of holes (h$^+$), superoxide ions ($\bullet$O$_2^-$), and hydroxyl radicals ($\bullet$OH), respectively [27,28]. As presented in Figure S9, the degradation efficiency of 4-CP decreased notably from 89.25% to 11.03% with the addition of NBT, suggesting the crucial role of $\bullet$O$_2^-$ in the photocatalytic degradation

process. Moreover, with the addition of IPA and EDTA, the degradation efficiency of 4-CP decreased to 75.3% and 51.67%, respectively. Herein, it could be concluded that $\bullet$OH, h^+, and $\bullet O_2^-$ played synergistic roles in the photocatalytic degradation of 4-CP, which was consistent with the EPR characterization (Figure S10).

2.2. Degradation Products and Pathways

To further analyze the photocatalytic degradation process of 4-CP, the intermediates were identified with the help of liquid chromatography coupled with mass spectrometry (LC-MS), and the possible degradation pathways of 4-CP are depicted in Figure 4a. The dichlorination and oxidation processes of 4-CP by h^+ and $\bullet O_2^-$ could produce p-benzoquinone (P1, m/z = 108), and the hydroxylation of 4-CP yielded 4-Chlorocatechol (P2, m/z = 143). Subsequently, the above intermediates under the attack of $\bullet$OH and $\bullet O_2^-$ were transferred into low-molecular-weight acids, including maleic acid (P3, m/z = 115) and malonic acid (P4, m/z = 103) [29–31]. Finally, it could be confirmed that these intermediates would fully break down to CO_2, H_2O, and Cl^- by the synergistic effects of h^+, $\bullet$OH, and $\bullet O_2^-$. The dechlorination efficiency of CQDs/$ZnIn_2S_4$-2 toward 4-CP could reach 84.4% (Figure S11). Moreover, the acute toxicity of 4-CP and its possible intermediates was evaluated using the Toxicity Estimation Software Tool (ECOSAR) according to the quantitative relationship of structure and activity. As depicted in Figure 4b, it is clear that the fish median lethal concentrations 50 (LC50s) of most intermediates were higher than that of 4-CP, suggesting the lower acute toxicity of intermediates than that of 4-CP [32,33]. DFT calculation was employed to optimize the structure of 4-CP (Figure 4c). The electrophilic (f^-), nucleophilic (f^+), and radical (f^0) Fukui indices could theoretically predict the attacked sites of 4-CP. As depicted in Figure 4d, the C_1, C_3, C_4, O_7, and Cl_8 (highlighted) with high values were more vulnerable to active radicals (h^+, $\bullet$OH, and $\bullet O_2^-$), which was consistent with the degradation pathways [34].

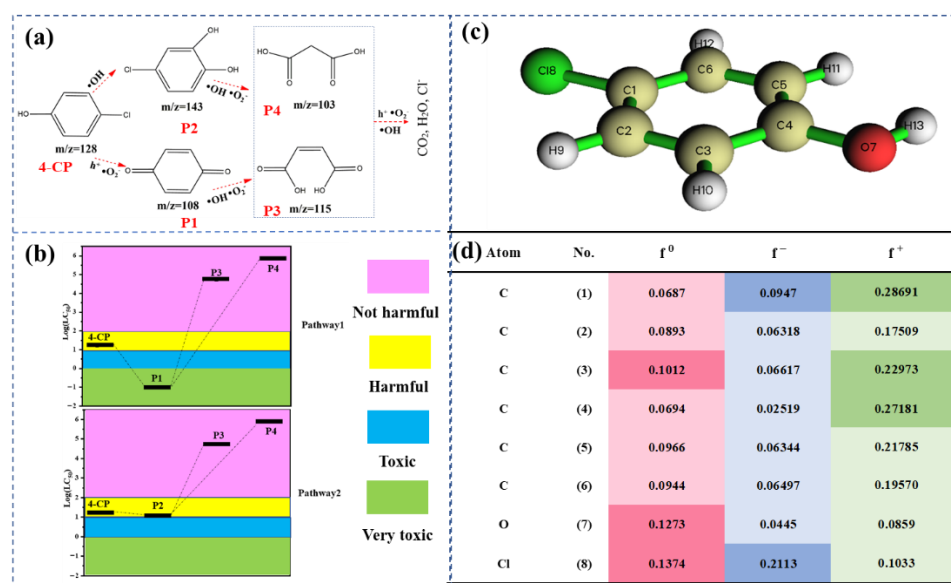**Figure 4.** (**a**) Photocatalytic degradation pathways of 4-CP; (**b**) acute toxicity LC_{50} of 4-CP and its possible intermediates; (**c**) molecular structural formula of 4-CP; and (**d**) calculated Fukui index of 4-CP.

2.3. Photocatalytic Mechanism

Based on the above analysis, the possible photocatalytic degradation mechanism of CQDs/$ZnIn_2S_4$-2 is schematically described in Figure 5. The band gap for $ZnIn_2S_4$ was 2.50 eV (Figure S12) [35]. Meanwhile, the potential of the conduction band for $ZnIn_2S_4$ was −1.02 eV (Figure S13). Herein, the potential of the valence band for $ZnIn_2S_4$ was calculated to be 1.48 eV [36]. Under simulated sunlight illustration, the electrons on the valence band

of $ZnIn_2S_4$ could migrate to its conduction band. Generally, the CQDs were regarded as an electron reservoir; thus, the electrons on the conduction band of $ZnIn_2S_4$ could migrate to the surface of CQDs. As the E_{CB} of $ZnIn_2S_4$ (−1.02 eV) was more negative than $E^\ominus$ $(O_2/\bullet O_2^-)$ (−0.33 eV), the photogenerated electrons could react with O_2 to generate $\bullet O_2^-$. Additionally, the E_{VB} of $ZnIn_2S_4$ (1.48 eV) was lower than that of $E^\ominus$ $(\bullet OH/OH^-)$ (2.24 eV), indicating that the $\bullet OH$ was derived from the electron-induced multistep reduction of O_2 instead of direct h^+ oxidation. Herein, in this study, the photocatalytic degradation of 4-CP involved the co-participation of $\bullet O_2^-$, $\bullet OH$, and h^+.
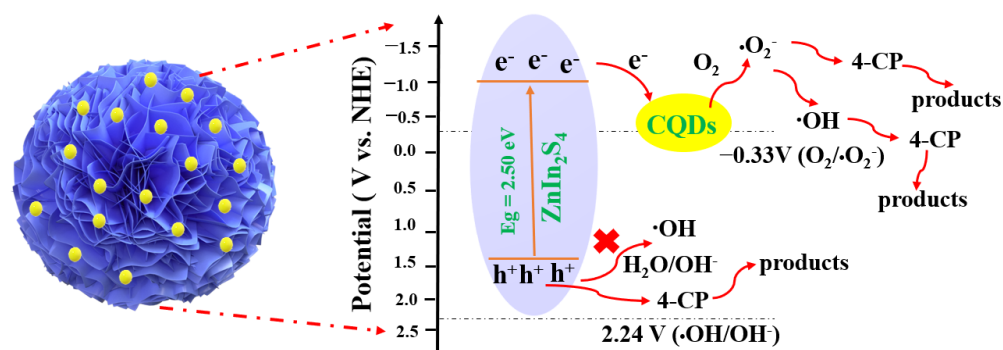

Figure 5. Degradation mechanism of CQDs/$ZnIn_2S_4$-2 toward 4-CP under Xe lamp irradiation.

3. Materials and Methods

3.1. Chemical Reagents

Zinc acetate dihydrate ($Zn(CH_3COO)_2 \cdot 2H_2O$)), indium(III) chloride ($InCl_3$), thioacetamide, isopropanol (IPA), nitroblue tetrazolium (NBT), and ethylene diamine tetraacetic acid (EDTA) were also purchased from Sinopharm Chemical Reagent Co., Ltd. (Shanghai, China). P-Chlorophenol (4-CP) was purchased from Aldrich. All chemicals were used as received.

3.2. Characterizations

The morphologies of CQDs/$ZnIn_2S_4$-2 were measured using a scanning electron microscope (SEM, Hitachi S-4800N, Tokyo, Japan) and high-resolution transmission electron microscope (HRTEM, JEOL JEM-2100F, Tokyo, Japan). The elemental mapping for CQDs/$ZnIn_2S_4$-2 was carried out using an energy dispersive spectrometer (EDS) equipped with the HRTEM. The crystalline structures of $ZnIn_2S_4$ and CQDs/$ZnIn_2S_4$-2 were obtained by X-ray diffraction (XRD) using a diffractometer (X'Pert Pro, PANalytical, Netherlands). X-ray photoelectron spectroscopy (XPS; AXIS ULTRA DLD, Kratos, London, UK) was used to analyze the chemical composition of CQDs/$ZnIn_2S_4$-2. UV–vis Diffuse Reflectance Spectroscopy (DRS) of $ZnIn_2S_4$ and CQDs/$ZnIn_2S_4$-2 was performed on an ultraviolet-visible (UV–Vis; Hitachi U-3900) spectrometer. The photocurrent responses, EIS curves, and Mott–Schottky curve of the fabricated photocatalysts were determined on an electrochemical workstation (CHI660E). The active species generated during photocatalytic processes were analyzed by electron paramagnetic spectroscopy (EPR, Bruker EMX 10/12, Oberkochen, Germany). The mineralization ability of photocatalysts was measured using a total organic carbon (TOC) analyzer (Shimadzu VCSN, Tokyo, Japan). The intermediates of 4-CP were identified by high-performance liquid chromatography–mass spectrometry (HPLC-MS, 1290 Infinity LC/6460 QQQ MS, Agilent, New York, NY, USA).

3.3. Materials Preparation

3.3.1. Synthesis of $ZnIn_2S_4$

$Zn(CH_3COO)_2 \cdot 2H_2O$ (0.5 mmol), $InCl_3$(1 mmol), and thioacetamide (2 mmol) were dissolved in water (60 mL) with continuous stirring for 30 min. Subsequently, the mixture was transferred into a Teflon-lined steel autoclave and maintained at 180 °C for 18 h. After

that, the collected precipitates were washed with ultrapure water several times. Finally, the obtained materials were dried in a vacuum at 60 °C overnight.

3.3.2. Synthesis of CQDs

Typically, a citric acid solution (0.2 mol/L, 200 mL, solution pH adjusted to 6.0 by $NH_3 \cdot H_2O$) was hydrothermally treated at 200 °C for 4 h. Subsequently, the obtained solution was treated with a 0.22 μm membrane filter and purified by dialysis for 48 h. Finally, the CQDs could be obtained after drying.

3.3.3. Synthesis of CQDs/ZnIn$_2$S$_4$-x

$Zn(CH_3COO)_2 \cdot 2H_2O$ (0.5 mmol), $InCl_3$ (1 mmol), and thioacetamide (2 mmol) were weighed and added to 60 mL of ultrapure water and then stirred at room temperature for 30 min. Then, the obtained CQDs with different amounts (1 wt%, 2 wt%, or 3 wt%) were added to the above solution and stirred for another 30 min. After that, the solution was then transferred to a Teflon-lined steel autoclave and treated at 180 °C for 18 h [37,38]. Finally, the products denoted as CQDs-ZnIn$_2$S$_4$-x (x = 1, 2, 3 wt%) were washed alternately with deionized water and absolute ethanol, and dried in a vacuum at 60 °C overnight.

3.4. Performance Evaluation

The photocatalytic reactivity of ZnIn$_2$S$_4$ and CQDs/ZnIn$_2$S$_4$-x was evaluated by the degradation of 4-CP under Xe lamp (500 W) irradiation. In a typical experiment, 0.01 g of the photocatalyst was dispersed in an aqueous solution of 4-CP (40 mL, 10 mg/L). Before the photocatalytic process, the solution was stirred in the dark for 30 min to reach the adsorption–desorption equilibrium. During the reaction process, 0.2 mL of solution was sampled and filtrated at each given interval for further analysis. High-performance liquid chromatography (HPLC; LC-20AT, Shimadzu, Japan) at a working wavelength of 281 nm was employed to obtain the concentration of 4-CP, and the flow rate was 1.0 mL/min. Furthermore, the mobile phase was a mixture of methanol and water ($V_{methanol}:V_{water}$ = 6:4). To measure the concentration of Cl^-, ion chromatography (Dionex ICS-3000, Oberkochen, Germany) was used. The eluent and regeneration solutions were 2% potassium hydroxide (100 mM KOH) and 98% Milli-Q water with a flow rate of 1.0 mL/min. The signals of ●OH, h^+, and ●O_2^- were determined on an electron paramagnetic resonance (EPR, Bruker EMX 10/12, Germany) spectrometer with 2,2,6, 6-tetramethylpiperidine oxide (TEMPO) and 5, 5-dimethyl-1-pyrroline N-oxide (DMPO) as the spin trap reagents.

4. Conclusions

To summarize, CQD-modified ZnIn$_2$S$_4$ nanoflowers were prepared by a facile hydrothermal method. The photocatalytic activities of the catalysts were explored under different reaction conditions using 4-CP as the target pollutant. The results confirmed that the CQDs/ZnIn$_2$S$_4$-x catalyst showed outstanding activity under Xe lamp irradiation, benefiting from the introduction of CQDs, which could not only enhance the absorption of visible light, but also serve as an efficient electron mediator to improve the activities of ZnIn$_2$S$_4$. The active species-trapping experiments and EPR characterization proved that ●O_2^-, ●OH and h^+ played a synergistic role in 4-CP degradation. This work opens a new method for the fabrication of high-activity photocatalysts that exhibit great potential in the fields of environmental remediation, energy conversion, and other relevant fields.

Supplementary Materials: The following supporting information can be downloaded at: https://www.mdpi.com/article/10.3390/catal12121545/s1, Figure S1: The HRTEM image of CQDs/ZnIn$_2$S$_4$-2; Figure S2: UV-vis absorption spectra of ZnIn$_2$S$_4$ and CQDs/ZnIn$_2$S$_4$-2; Figure S3: The pseudo-first-order reaction kinetics; Figure S4: TOC removal efficiency of 4-CP by ZnIn$_2$S$_4$ and CQDs/ZnIn$_2$S$_4$-2; Figure S5: Effect of initial pH value for 4-CP degradation on CQDs/ZnIn$_2$S$_4$-2; Figure S6: Effect of catalyst concentration on 4-CP degradation; Figure S7: Effect of inorganic anions for 4-CP degradation on CQDs/ZnIn$_2$S$_4$-2; Figure S8: XRD pattern of CQDs/ZnIn$_2$S$_4$-2 after used; Figure S9: Trapping experiment of active species for photocatalytic degradation of 4-CP; Figure S10: EPR spectra

of CQDs/ZnIn$_2$S$_4$-2 in methanol dispersion for DMPO-•O$_2^-$ (a), water dispersion for DMPO-•OH (c) and TEMPO-h$^+$ (b) under Xe lamp irradiation.; Figure S11: Cl$^-$ concentration of 4-CP; Figure S12: The band gap of ZnIn$_2$S$_4$; Figure S13: Mott-Schottky plot of ZnIn$_2$S$_4$; Table S1: Comparison of 4-CP degradation performance of this work and reported photocatalysts [7,39–41].

Author Contributions: Writing, preparation and characterization of materials, and editing, J.Q. and Q.L.; editing and validation, Y.Q.; supervision, F.L. and F.W. All authors have read and agreed to the published version of the manuscript.

Data Availability Statement: The processed data required to reproduce these findings are available by e-mail to the corresponding author.

Conflicts of Interest: The authors declare no conflict of interest.

References

1. Yang, K.C.; Zhao, Y.X.; Ji, M.; Li, Z.L.; Zhai, S.Y.; Zhou, X.; Wang, Q.; Wang, C.; Liang, B. Challenges and opportunities for the biodegradation of chlorophenols: Aerobic, anaerobic and bioelectrochemical processes. *Water Res.* **2021**, *193*, 116862. [CrossRef] [PubMed]
2. Xu, L.J.; Wang, J.L. Fenton-like degradation of 2,4-dichlorophenol using Fe$_3$O$_4$ magnetic nanoparticles. *Appl. Catal. B* **2012**, *123*, 117–126. [CrossRef]
3. Wang, M.L.; Fang, G.D.; Liu, P.; Zhou, D.M.; Ma, C.; Zhang, D.J.; Zhan, J.H. Fe$_3$O$_4$@beta-CD nanocomposite as heterogeneous Fenton-like catalyst for enhanced degradation of 4-chlorophenol (4-CP). *Appl. Catal. B* **2016**, *188*, 113–122. [CrossRef]
4. Valadez-Renteria, E.; Barrera-Rendon, E.; Oliva, J.; Rodriguez-Gonzalez, V. Flexible CuS/TiO$_2$ based composites made with recycled bags and polystyrene for the efficient removal of the 4-CP pesticide from drinking water. *Sep. Purif. Technol.* **2021**, *270*, 118821. [CrossRef]
5. Song, R.; Chi, H.B.; Ma, Q.L.; Li, D.F.; Wang, X.M.; Gao, W.S.; Wang, H.; Wang, X.L.; Li, Z.L.; Li, C. Highly Efficient Degradation of Persistent Pollutants with 3D Nanocone TiO$_2$-Based Photoelectrocatalysis. *J. Am. Chem. Soc.* **2021**, *143*, 13664–13674. [CrossRef]
6. Peng, Y.Q.; Chen, J.H.; Lu, S.Y.; Huang, J.X.; Zhang, M.M.; Buekens, A.; Li, X.D.; Yan, J.H. Chlorophenols in Municipal Solid Waste Incineration: A review. *Chem. Eng. J.* **2016**, *292*, 398–414. [CrossRef]
7. Liu, J.; Han, D.D.; Chen, P.J.; Zhai, L.P.; Wang, Y.J.; Chen, W.H.; Mi, L.W.; Yang, L.P. Positive roles of Br in g-C$_3$N$_4$/PTCDI-Br heterojunction for photocatalytic degrading chlorophenols. *Chem. Eng. J.* **2021**, *418*, 129492. [CrossRef]
8. Gong, Q.J.; Liu, Y.; Dang, Z. Core-shell structured Fe$_3$O$_4$@GO@MIL-100(Fe) magnetic nanoparticles as heterogeneous photo-Fenton catalyst for 2,4-dichlorophenol degradation under visible light. *J. Hazard. Mater.* **2019**, *371*, 677–686. [CrossRef]
9. Ding, M.; Zhou, J.J.; Yang, H.C.; Cao, R.Y.; Zhang, S.W.; Shao, M.H.; Xu, X.J. Synthesis of Z-scheme g-C$_3$N$_4$ nanosheets/Ag$_3$PO$_4$ photocatalysts with enhanced visible-light photocatalytic performance for the degradation of tetracycline and dye. *Chin. Chem. Lett.* **2020**, *31*, 71–76. [CrossRef]
10. Hu, D.H.; Song, L.J.; Yan, R.; Li, Z.J.; Zhang, Z.Q.; Sun, J.H.; Bian, J.; Qu, Y.; Jing, L.Q. Valence-mixed iron phthalocyanines/(100) Bi$_2$MoO$_6$ nanosheet Z-scheme heterojunction catalysts for efficient visible-light degradation of 2-chloro-phenol via preferential dechlorination. *Chem. Eng. J.* **2022**, *440*, 135786. [CrossRef]
11. Yadav, G.; Ahmaruzzaman, M. ZnIn$_2$S$_4$ and ZnIn$_2$S$_4$ based advanced hybrid materials: Structure, morphology and applications in environment and energy. *Inorg. Chem. Commun.* **2022**, *138*, 109288. [CrossRef]
12. Yuan, D.L.; Sun, M.T.; Tang, S.F.; Zhang, Y.T.; Wang, Z.T.; Qi, J.B.; Rao, Y.D.; Zhang, Q.R. All-solid-state BiVO$_4$/ZnIn$_2$S$_4$ Z-scheme composite with efficient charge separations for improved visible light photocatalytic organics degradation. *Chin. Chem. Lett.* **2020**, *31*, 547–550. [CrossRef]
13. Liu, Q.; Lu, H.; Shi, Z.W.; Wu, F.L.; Guo, J.; Deng, K.M.; Li, L. 2D ZnIn$_2$S$_4$ Nanosheet/lD TiO$_2$ Nanorod Heterostructure Arrays for Improved Photoelectrochemical Water Splitting. ACS Appl. *Mater. Inter.* **2014**, *6*, 17200–17207. [CrossRef] [PubMed]
14. Li, W.J.; Lin, Z.Y.; Yang, G.W. A 2D self-assembled MoS$_2$/ZnIn$_2$S$_4$ heterostructure for efficient photocatalytic hydrogen evolution. *Nanoscale* **2017**, *9*, 18290–18298. [CrossRef] [PubMed]
15. Gong, G.; Liu, Y.H.; Mao, B.D.; Tan, L.L.; Yang, Y.L.; Shi, W.D. Ag doping of Zn-In-S quantum dots for photocatalytic hydrogen evolution: Simultaneous bandgap narrowing and carrier lifetime elongation. *Appl. Catal. B* **2017**, *216*, 11–19. [CrossRef]
16. Zuo, G.C.; Wang, Y.T.; Teo, W.L.; Xian, Q.M.; Zhao, Y.L. Direct Z-scheme TiO$_2$-ZnIn$_2$S$_4$ nanoflowers for cocatalyst-free photocatalytic water splitting. *Appl. Catal. B* **2021**, *291*, 120126. [CrossRef]

17. Lai, J.H.; Jiang, X.Y.; Zhao, M.; Cui, S.A.; Yang, J.; Li, Y.F. Thickness-dependent layered $BiOIO_3$ modified with carbon quantum dots for photodegradation of bisphenol A: Mechanism, pathways and DFT calculation. *Appl. Catal. B* **2021**, *298*, 120622. [CrossRef]

18. Ren, P.; Fu, X.B.; Zhang, Y.M. Carbon Quantum Dots-TiO_2 Nanocomposites with Enhanced Catalytic Activities for Selective Liquid Phase Oxidation of Alcohols. *Catal. Lett.* **2017**, *147*, 1679–1685. [CrossRef]

19. Liu, S.Y.; Li, X.; Meng, X.; Chen, T.X.; Kong, W.Y.; Li, Y.; Zhao, Y.X.; Wang, D.W.; Zhu, S.M.; Cheema, W.A.; et al. Enhanced visible/near-infrared light harvesting and superior charge separation via 0D/2D all-carbon hybrid architecture for photocatalytic oxygen evolution. *Carbon* **2020**, *167*, 724–735. [CrossRef]

20. Fu, Y.K.; Zeng, G.M.; Lai, C.; Huang, D.L.; Qin, L.; Yi, H.; Liu, X.G.; Zhang, M.M.; Li, B.S.; Liu, S.Y. Hybrid architectures based on noble metals and carbon-based dots nanomaterials: A review of recent progress in synthesis and applications. *Chem. Eng. J.* **2020**, *399*, 125743. [CrossRef]

21. Yu, H.B.; Huang, J.H.; Jiang, L.B.; Shi, Y.H.; Yi, K.X.; Zhang, W.; Zhang, J.; Chen, H.Y.; Yuan, X.Z. Enhanced photocatalytic tetracycline degradation using N-CQDs/O_V-BiOBr composites. *Chem. Eng. J.* **2020**, *402*, 126187. [CrossRef]

22. Jiang, C.L.; Wang, H.; Wang, Y.Q.; Ji, H.B. All solid-state Z-scheme CeO_2/$ZnIn_2S_4$ hybrid for the photocatalytic selective oxidation of aromatic alcohols coupled with hydrogen evolution. *Appl. Catal. B* **2020**, *277*, 119235. [CrossRef]

23. Shao, Y.Q.; Dou, Z.L.; Liang, X.Y.; Zhang, X.X.; Ji, M.; Pang, M.; Wang, M.; Wang, X.K. $ZnIn_2S_4$ nanosheet growth on amine-functionalized SiO_2 for the photocatalytic reduction of CO_2. *Catal. Sci. Technol.* **2022**, *12*, 606–612. [CrossRef]

24. Sin, J.C.; Lam, S.M.; Zeng, H.H.; Lin, H.; Li, H.X.; Huang, L.L.; Tham, K.O.; Mohamed, A.R.; Lim, J.W. Enhanced synchronous photocatalytic 4-chlorophenol degradation and Cr (VI) reduction by novel magnetic separable visible-light-driven Z-scheme $CoFe_2O_4$/P-doped BiOBr heterojunction nanocomposites. *Environ. Res.* **2022**, *212*, 113394. [CrossRef]

25. Xu, X.; Wang, J.; Chen, T.; Yang, N.; Wang, S.Y.; Ding, X.; Chen, H. Deep insight into ROS mediated direct and hydroxylated dichlorination process for efficient photocatalytic sodium pentachlorophenate mineralization. *Appl. Catal. B* **2021**, *296*, 120352. [CrossRef]

26. Xiang, X.F.; Wu, L.Y.; Zhu, J.J.; Li, J.Z.; Liao, X.; Huang, H.C.; Fan, J.J.; Lv, K.L. Photocatalytic degradation of sulfadiazine in suspensions of TiO_2 nanosheets with exposed (001) facets. *Chin. Chem. Lett.* **2021**, *32*, 3215–3220. [CrossRef]

27. Huang, S.H.; Wang, Y.; Wan, J.Q.; Yan, Z.C.; Ma, Y.W.; Zhang, G.H.; Wang, S.L. $Ti_3C_2T_x$ as electron-hole transfer mediators to enhance AgBr/BiOBr Z heterojunction photocatalytic for the degradation of Tetrabromobisphenol A: Mechanism Insight. *Appl. Catal. B* **2022**, *319*, 121913. [CrossRef]

28. Qin, C.D.; Tang, J.J.; Qiao, R.X.; Lin, S.J. Tetracycline sensitizes TiO_2 for visible light photocatalytic degradation via ligand-to-metal charge transfer. *Chin. Chem. Lett.* **2022**, *33*, 5218–5222. [CrossRef]

29. Xu, X.J.; Tang, D.D.; Cai, J.H.; Xi, B.D.; Zhang, Y.; Pi, L.; Mao, X.H. Heterogeneous activation of peroxymonocarbonate by chalcopyrite ($CuFeS_2$) for efficient degradation of 2,4-dichlorophenol in simulated groundwater. *Appl. Catal. B* **2019**, *251*, 273–282. [CrossRef]

30. Huang, S.N.; Tian, F.; Dai, J.W.; Tian, X.S.; Li, G.F.; Liu, Y.L.; Chen, Z.Q.; Chen, R. Highly efficient degradation of chlorophenol over bismuth oxides upon near-infrared irradiation: Unraveling the effect of Bi-O-Bi-O defects cluster and O-1(2) involved process. *Appl. Catal. B* **2021**, *298*, 120576. [CrossRef]

31. Wang, Q.; Jiang, Y.; Yang, S.R.; Lin, J.Y.; Lu, J.H.; Song, W.; Zhu, S.J.; Wang, Z.H. Selective degradation of parachlorophenol using Fe/Fe_3O_4@CPPy nanocomposites via the dual nonradical/radical peroxymonosulfate activation mechanisms. *Chem. Eng. J.* **2022**, *445*, 136806. [CrossRef]

32. Ge, T.T.; Han, J.Y.; Qi, Y.M.; Gu, X.Y.; Ma, L.; Zhang, C.; Naeem, S.; Huang, D.J. The toxic effects of chlorophenols and associated mechanisms in fish. *Aquat. Toxicol.* **2017**, *184*, 78–93. [CrossRef] [PubMed]

33. Zhang, B.; Ma, J.; Chi, H.Z.; Ding, A.; Xin, Y.J.; Ma, Y.Y.; Liu, Q.L.; He, X. Novel VUV/g-C_3N_4 system with high adaptability to varied environmental conditions and outstanding degradation capacity for chlorophenols. *J. Hazard. Mater.* **2021**, *419*, 126473. [CrossRef]

34. Wang, A.W.; Ni, J.X.; Wang, W.; Liu, D.M.; Zhu, Q.; Xue, B.X.; Chang, C.C.; Ma, J.; Zhao, Y. MOF Derived Co-Fe nitrogen doped graphite carbon@crosslinked magnetic chitosan Micro-nanoreactor for environmental applications: Synergy enhancement effect of adsorption-PMS activation. *Appl. Catal. B* **2022**, *319*, 121926. [CrossRef]

35. Li, X.Q.; Chen, D.Y.; Li, N.J.; Xu, Q.F.; Li, H.; He, J.H.; Lu, J.M. Hollow SnO_2 nanotubes decorated with $ZnIn_2S_4$ nanosheets for enhanced visible-light photocatalytic activity. *J. Alloy Compd.* **2020**, *843*, 155772. [CrossRef]

36. Zada, A.; Khan, M.; Khan, M.A.; Khan, Q.; Habibi-Yangjeh, A.; Dang, A.; Maqbool, M. Review on the hazardous applications and photodegradation mechanisms of chlorophenols over different photocatalysts. *Environ. Res.* **2021**, *195*, 110742. [PubMed]

37. Liu, B.B.; Liu, X.J.; Li, L.; Li, J.W.; Li, C.; Gong, Y.Y.; Niu, L.Y.; Zhao, X.S.; Sun, C.Q. $ZnIn_2S_4$ flowerlike microspheres embedded with carbon quantum dots for efficient photocatalytic reduction of Cr(VI). *Chin. J. Catal.* **2018**, *39*, 1901–1909. [CrossRef]

38. Xu, H.Q.; Jiang, Y.H.; Yang, X.Y.; Li, F.; Li, A.P.; Liu, Y.; Zhang, J.M.; Zhou, Z.Z.; Ni, L. Fabricating carbon quantum dots doped $ZnIn_2S_4$ nanoflower composites with broad spectrum and enhanced photocatalytic Tetracycline hydrochloride degradation. *Mater. Res. Bull.* **2018**, *97*, 158–168. [CrossRef]

39. Di, J.; Xia, J.; Yin, S.; Xu, H.; Xu, L.i.; Xu, Y.; He, M.; Li, H. Preparation of sphere-like g-C_3N_4/BiOI photocatalysts via a reactable ionic liquid for visible-light-driven photocatalytic degradation of pollutants. *J. Mater. Chem. A* **2014**, *2*, 5340. [CrossRef]

40. Wang, J.; Xia, Y.i.; Zhao, H.; Wang, G.; Xiang, L.; Xu, J.; Komarneni, S. Oxygen defectsmediated Z-scheme charge separation in g-C$_3$N$_4$/ZnO photocatalysts for enhanced visible-light degradation of 4-chlorophenol and hydrogen evolution. *Appl. Catal. B Environ.* **2017**, *206*, 406–416. [CrossRef]

41. Ismael, M.; Elhaddad, E.; Taffa, D.H.; Wark, M. Solid state route for synthesis of YFeO$_3$/g-C$_3$N$_4$ composites and its visible light activity for degradation of organic pollutants. *Catal. Today* **2018**, *313*, 47–54. [CrossRef]